Ero1-α and PDIs constitute a hierarchical electron transfer network of endoplasmic reticulum oxidoreductases

Kazutaka Araki,[1,2] Shun-ichiro Iemura,[3] Yukiko Kamiya,[4,5] David Ron,[6,7] Koichi Kato,[4,5,8] Tohru Natsume,[1] and Kazuhiro Nagata[2]

[1]Molecular Profiling Research Center for Drug Discovery, National Institute of Advanced Industrial Science and Technology, Koto-ku, Tokyo 135-0064, Japan
[2]Laboratory of Molecular and Cellular Biology, Faculty of Life Sciences, Kyoto Sangyo University, Kita-ku, Kyoto 603-8047, Japan
[3]Innovative drug development translational research section, Fukushima Medical University, Fukushima 960-1295, Japan
[4]Institute for Molecular Science and Okazaki Institute for Integrative Bioscience, National Institutes of Natural Sciences, Okazaki 444-8787, Japan
[5]Graduate School of Pharmaceutical Sciences, Nagaya City University, Nagoya 467-8603, Japan
[6]Metabolic Research Laboratories; and [7]National Institute for Health Research Cambridge Biomedical Research Centre, Addenbrooke's Hospital; University of Cambridge, Cambridge CB2 0QQ, England, UK
[8]The Glycoscience Institute, Ochanomizu University, Tokyo 112-8610, Japan

Ero1-α and endoplasmic reticulum (ER) oxidoreductases of the protein disulfide isomerase (PDI) family promote the efficient introduction of disulfide bonds into nascent polypeptides in the ER. However, the hierarchy of electron transfer among these oxidoreductases is poorly understood. In this paper, Ero1-α–associated oxidoreductases were identified by proteomic analysis and further confirmed by surface plasmon resonance. Ero1-α and PDI were found to constitute a regulatory hub, whereby PDI induced conformational flexibility in an Ero1-α shuttle cysteine (Cys99) facilitated intramolecular electron transfer to the active site. In isolation, Ero1-α also oxidized ERp46, ERp57, and P5; however, kinetic measurements and redox equilibrium analysis revealed that PDI preferentially oxidized other oxidoreductases. PDI accepted electrons from the other oxidoreductases via its a′ domain, bypassing the a domain, which serves as the electron acceptor from reduced glutathione. These observations provide an integrated picture of the hierarchy of cooperative redox interactions among ER oxidoreductases in mammalian cells.

Introduction

Membrane and secretory proteins are co-translationally transported into the ER and folded with the assistance of a series of chaperones, glycosylation enzymes, and oxidoreductases (Hebert and Molinari, 2007; Araki and Nagata, 2011b). Oxidoreductases in the ER ensure the efficient formation of native disulfide bonds during the folding of nascent polypeptides. The best-characterized ER oxidoreductase is protein disulfide isomerase (PDI; Freedman et al., 1994). PDI contains two thioredoxin domains, each of which contains a CXXC motif involved in dithiol–disulfide exchange reactions. PDI introduces disulfide bonds into nascent proteins as an oxidoreductase, rearranges incorrect disulfide bonds as an isomerase, and assists the folding of and prevents the aggregation of unfolded proteins as a molecular chaperone. In addition to PDI, more than 20 oxidoreductases have been identified in the mammalian ER, including ERp57, ERp44, ERp72, ERdj5, P5, and ERp46, each of which contains at least one thioredoxin-like domain (Ellgaard and Ruddock, 2005; Hatahet and Ruddock, 2009). Although some ER oxidoreductases have well-characterized specific functions (Appenzeller-Herzog and Ellgaard, 2008; Rutkevich et al., 2010; Benham, 2012), the biological implications of the diversity of ER oxidoreductases remains to be investigated.

PDI is generally thought to be the primary acceptor of oxidative equivalents from the Ero1 family of oxidases, whereas

Correspondence to Kazuhiro Nagata: nagata@cc.kyoto-su.ac.jp

Y. Kamiya's present address is Graduate School of Engineering, Nagoya University, Chikusa-ku, Nagoya 464-8603, Japan.

Abbreviations used in this paper: CBB, Coomassie brilliant blue; NEM, *N*-ethylmaleimide; NMR, nuclear magnetic resonance; PDI, protein disulfide isomerase; SPR, surface plasmon resonance; WT, wild type.

The Rockefeller University Press $30.00
J. Cell Biol. Vol. 202 No. 6 861–874
www.jcb.org/cgi/doi/10.1083/jcb.201303027

the actual order of electron transfer among oxidoreductases remains to be established (Riemer et al., 2009; Araki and Inaba, 2012). Although Prx4 and vitamin K epoxide reductase were recently shown to play an auxiliary role in ER oxidative folding in mammalian cells, the Ero1 enzymes are the best-conserved ER oxidases and quantitatively dominate oxidation in the ER (Appenzeller-Herzog et al., 2010; Zito et al., 2010; van Lith et al., 2011; Araki and Inaba, 2012; Rutkevich and Williams, 2012). Recent evidence shows that PDI regulates Ero1-α activity by catalyzing the rearrangement of the regulatory cysteine pairs of Ero1-α (Araki and Inaba, 2012). Thus, PDI and Ero1-α constitute a feedback regulatory system that responds to the redox conditions of the ER (Sevier and Kaiser, 2008; Appenzeller-Herzog et al., 2010). However, the significance of the interaction of PDI with Ero1-α and role of other oxidoreductases in the disulfide transfer chain promoting efficient oxidation of nascent polypeptides in the ER needs to be further defined. Here, we present a systematic study of the kinetic interactions of Ero1-α with various ER oxidoreductases to reveal their regulatory network and molecular mechanisms.

Results

Ero1-α binds to ER-resident oxidoreductases

Ero1-α–interacting partners have been previously identified (see Table S1 and references therein). But here, we attempted to acquire a comprehensive dataset. FLAG-tagged Ero1-α was expressed in HEK293T cells, and the Ero1-α–associated proteins in the anti-FLAG antibody immunoprecipitates were analyzed by liquid chromatography coupled with tandem mass spectrometry (Fig. S1 A; Natsume et al., 2002). Most of the peptides recovered in complex with Ero1-α were derived from ER-resident soluble oxidoreductases, including PDI, ERp44, ERp57, ERp72, ERp46, and P5. The interactions were confirmed by immunoblotting experiments, in which immunoprecipitates from cells stably expressing FLAG-tagged Ero1-α were probed with antibodies to the oxidoreductases (Fig. 1 A). The interactions with endogenous Ero1-α were further confirmed by immunoprecipitation after transient overexpression of the tagged oxidoreductases (Fig. S1 B). Of note, active site CXXA mutants of the oxidoreductases showed the strongest interactions with Ero1-α, as demonstrated previously (Table S1; Anelli et al., 2003; Jessop et al., 2007, 2009a). Because the CXXA mutant reportedly prolongs the mixed disulfide intermediate states, these results suggest that the CXXC active sites are involved in interactions between Ero1-α and oxidoreductases (Hatahet and Ruddock, 2007; Jessop et al., 2009b).

Direct interactions of Ero1-α with the aforementioned identified oxidoreductases were assayed by surface plasmon resonance (SPR) with immobilized Ero1-α and soluble oxidoreductases under redox conditions equivalent to those in the ER: a reduced glutathione (GSH) to oxidized glutathione (GSSG) ratio of 4:1 (Fig. S1 C; Dixon et al., 2008; Araki and Nagata, 2011a). A two-state model was adopted to calculate the association and dissociation rate constants with the first equilibrium constants (Fig. S1 D). These values are shown in Fig. 1 B, in which the diagonal lines represent the dissociation constants (K_d). PDI clearly showed the strongest binding to Ero1-α with a K_d of ∼1.7 μM, which is consistent with the previously reported value (Table S1; Wang et al., 2009; Inaba et al., 2010; Araki and Nagata, 2011a; Masui et al., 2011). Ero1-α showed sequentially decreasing binding affinities to ERp44, P5, and ERp57/ERp72, and its affinity to ERp46 was the weakest. Furthermore, the binding kinetics of PDI were almost identical under different redox buffers, suggesting the interaction analyzed by SPR is independent of thiol exchange (unpublished data).

Ero1-α oxidizes oxidoreductases in vitro

To elucidate the functional significance of these interactions of Ero1-α with other oxidoreductases, we adopted an oxygen consumption assay to monitor the oxidation by Ero1-α in the presence of GSH as the upstream electron donor, as Ero1-α transfers the pair of electrons recovered from PDI to molecular oxygen, resulting in oxygen consumption that can be monitored by an oxygen-specific electrode (Fig. 1 C; Gross et al., 2006). Oxygen consumption was not observed in the absence of an oxidoreductase (Fig. S1 E, black line), which indicates that Ero1-α inefficiently oxidizes GSH. Addition of PDI markedly stimulated oxygen consumption as previously reported (Fig. S1 E, blue line; Baker et al., 2008; Inaba et al., 2010; Araki and Nagata, 2011a).

Ero1-α activity is known to be accelerated by reduced substrate, most probably PDI, through the reduction or isomerization of regulatory disulfides (Fig. S1 F; Sevier et al., 2007; Appenzeller-Herzog et al., 2008; Tavender and Bulleid, 2010). To prevent this factor from affecting the rate of enzymatic activity, we used a constitutively active Ero1-α(C104A/C131A) (Baker et al., 2008; Araki and Nagata, 2011a). In the presence of PDI, the mutant Ero1-α consumed oxygen faster than the wild-type (WT) enzyme, as expected (Fig. S1 E, compare blue and red lines).

A similar acceleration of oxygen consumption by the constitutively active Ero1-α(C104A/C131A) was also observed upon incubation with other oxidoreductases (ERp46, ERp57, and P5), indicating that the constitutively active Ero1-α(C104A/C131A) possesses oxidase activity against these ER oxidoreductases (compare Fig. 1, D and E; Inaba et al., 2010). Interestingly, the rank order of oxygen consumption by the oxidoreductases was not perfectly correlated with their binding affinities, with the lower affinity ERp46 exhibiting higher rates of oxygen consumption than other oxidoreductases. ERp72 showed unique characteristics by exerting a negligible effect on oxygen consumption by Ero1-α, although it did physically interact with Ero1-α (Fig. 1, D and E). In summary, Ero1-α exhibited the strongest physical and catalytic interaction with PDI, which is probably caused by the sterically optimized interaction oriented by the β hairpin of Ero1-α and the hydrophobic pocket in the b′ domain of PDI (Masui et al., 2011).

Ero1-α is dominantly regulated by PDI

Activated Ero1-α has a potential to oxidize other oxidoreductases, whereas WT Ero1-α only oxidizes PDI (Fig. 1, D and E). This result suggests that PDI could activate Ero1-α most efficiently and PDI was in turn oxidized by the activated Ero1-α. To address this point, we examined the activation of Ero1-α by the

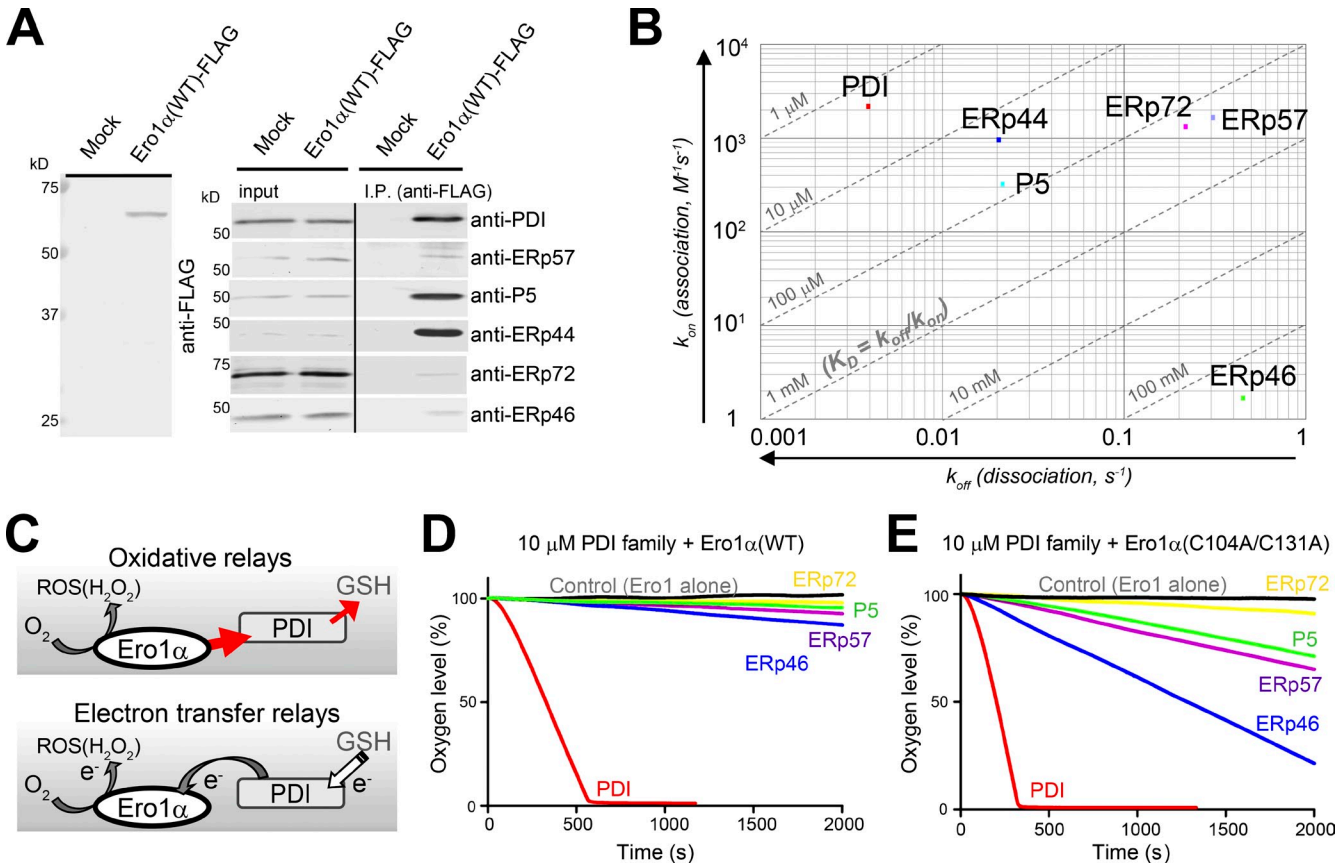

Figure 1. **Ero1-α binds to ER-resident oxidoreductases and preferentially oxidizes PDI.** (A, left) HEK293T cells (Mock) or HEK293T cells stably expressing Ero1-α–FLAG (Ero1-α(WT)–FLAG) were lysed and subjected to immunoprecipitation (I.P.) using antibodies against FLAG. (right) Resulting precipitates were examined by immunoblot analysis with the indicated antibodies. The black line on the right indicates the removal of intervening lanes for presentation purposes. (B) Association or dissociation rate constants (k_{on} or k_{off}) were determined with a two-state reaction model, and their first equilibrium constants are plotted. Diagonal lines represent dissociation constants (K_d). Data represent means from at least four individual experiments (see also Fig. S1, C and D). (C) Schematic models of oxidative relays (top) and electron transfer relays (bottom) between Ero1-α and PDI. (D) Assays were conducted in a sealed chamber starting with air-saturated buffer containing 10 mM GSH, which was regarded as the 100% oxygen level (~250 μM oxygen). Control experiments are shown in Fig. S1 E. (D and E) Oxidation of reduced oxidoreductases was initiated by the injection of 2 μM Ero1-α (D) or Ero1-α(C104A/C131A) (E) and was monitored with an oxygen electrode. ROS, reactive oxygen species.

different oxidoreductases through the overexpression or knockdown of these proteins (Table S1; Appenzeller-Herzog et al., 2008). The O_{X1} (active) and O_{X2} (inactive) forms of endogenous Ero1-α can be separated by using nonreducing gels (Fig. S1 E; Benham et al., 2000; Appenzeller-Herzog et al., 2008). The $O_{X1}/(O_{X2} + O_{X1})$ ratio of endogenous Ero1-α was increased by the overexpression of PDI (Fig. 2 A) and decreased by siRNA-mediated PDI knockdown (Fig. 2 B and Fig. S2 A). This finding indicated that PDI could alter the activity of Ero1-α, which is consistent with a previous study (Appenzeller-Herzog et al., 2008).

Mutants of full-length PDI were created, in which the cysteines in the CXXC motif in either the a or a′ catalytic thioredoxin domains was mutated to serine (PDI(a′) or PDI(a), respectively; Fig. 2 C). Both mutants were impaired in affecting the $O_{X1}/(O_{X2} + O_{X1})$ ratio, with PDI(a) having essentially no activity, indicating that both domains of PDI contribute to the efficient activation of Ero1-α (Fig. 2 A). These observations are consistent with previous experiments, suggesting the intramolecular transfer of electrons from the a domain to the a′ domain within PDI during its oxidation by Ero1-α (Araki and Nagata, 2011a).

Overexpression or siRNA-mediated down-regulation of other oxidoreductases, including ERp57, ERp72, and ERp44, had no significant effect on the $O_{X1}/(O_{X2} + O_{X1})$ ratio (Fig. 2, A and B). Whereas the overexpression of ERp46 or P5 had a modest effect (Fig. 2 A), down-regulation of either of these oxidoreductases caused negligible changes in the $O_{X1}/(O_{X2} + O_{X1})$ ratio (Fig. 2 B). Collectively, these results demonstrate that PDI is the major regulator of Ero1-α activity, whereas other oxidoreductases contribute modestly, if at all, to such regulation.

The flexibility of Cys99 of Ero1-α is accelerated by its interaction with PDI

To explore in further detail the Ero1-α–PDI interaction, we adopted nuclear magnetic resonance (NMR) analysis to investigate the effect of the interaction with PDI on the molecular dynamics of Ero1-α. It is technically difficult to analyze the entire three-dimensional conformation of Ero1-α by NMR because of its molecular size (~54 kD in the free form and ~110 kD in the complex with PDI). Given that cysteine residues are involved in the electron relays and their states will reflect the activity of Ero1-α, we prepared the constitutively active Ero1-α(C104A/C131A) in

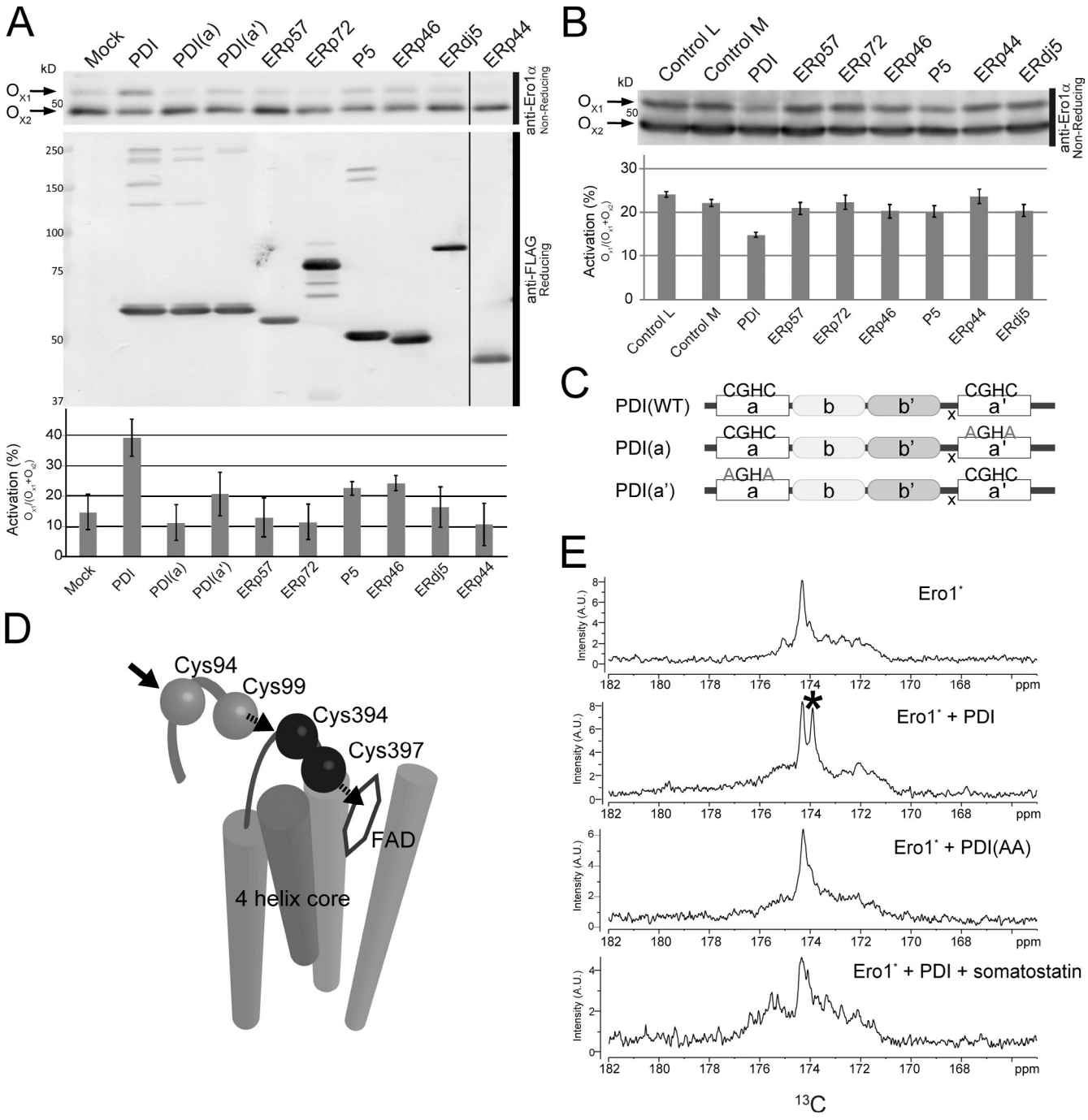

Figure 2. **PDI dominantly alters the activity of endogenous Ero1-α and increases conformational flexibility in a shuttle cysteine, Cys99, of Ero1-α.** (A and B) HEK293T cells in which the series of oxidoreductases was overexpressed for 24 h (A) or knocked down for 72 h (B) were trapped by alkylation with NEM and solubilized in lysis buffer. The supernatant was subjected to precipitation with Con A–Sepharose, and the glycoprotein fraction was analyzed by immunoblot analysis with the anti–Ero1-α antibody under nonreducing condition. Black lines indicate the removal of intervening lanes for presentation purposes. As controls, cells were transfected with mock vector or two different siRNAs (L, low GC content; M, medium GC content). The activated states of Ero1-α (O_{x1}/ (O_{x1} + O_{x2})) were quantified as shown in the bottom graphs of Fig. 2 (A and B). Mutants of full-length PDI containing only the intact a or intact a′ catalytic thioredoxin domain are shown as PDI(a) and PDI(a′), respectively (see also Fig. 2 C). Data represent means ± SDs from three independent experiments (see also Fig. S2 A). Although we have reported that ERdj5 works as a reductase in the ER-associated degradation process, it had almost no significant effect on the redox states of Ero1-α (Ushioda et al., 2008). (C) Schematic representation of human PDI proteins with the CGHC active sites and the mutated AGHA sites indicated. x denotes a linker region between the b′ and the a′ domain. (D) Schematic and simplified model of Ero1-α and its intramolecular electron flow (Araki and Inaba, 2012). Four spheres show the catalytically essential cysteines, two of which form the shuttle disulfide (light gray, Cys94-Cys99) on the flexible loop. The other cysteines form active site disulfides (dark gray, Cys394-Cys397) located proximally to the cofactor (flavin

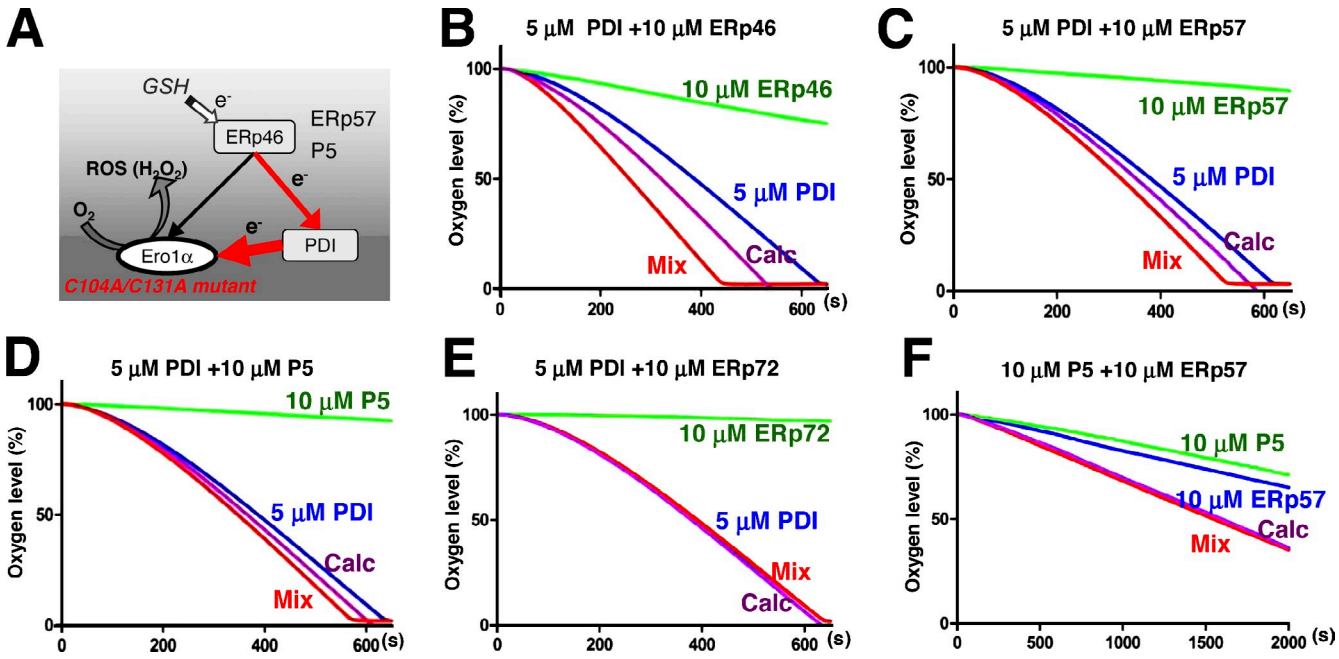

Figure 3. **Synergistic effects of oxidoreductases (ERp46, ERp57, and P5) on oxygen consumption in the presence of PDI and constitutively active Ero1-α.** (A) Schematic model of intermolecular electron flow among oxidoreductases. (B–E) Oxygen consumption was assayed in the presence of 10 mM GSH and 10 μM ERp46 (B), ERp57 (C), P5 (D), and ERp72 (E) with or without 5 μM PDI. Calc represents calculated data from individual consumption rates of the oxidoreductases. Mix represents actual consumption rates under conditions in which 10 μM of each oxidoreductase and 5 μM PDI were mixed in the presence of 10 mM GSH. (F) 10 μM P5 and 10 μM ERp57, without PDI, were mixed in the presence of 10 mM GSH. ROS, reactive oxygen species.

which the carbonyl carbon of cysteine was selectively labeled with ^{13}C and examined whether the NMR signals originating from cysteines were affected by the presence or absence of PDI. After subtracting the background signals derived from natural isotope abundance, several peaks were notably detected. A selective double-labeling method was used to assign the sharp peak; the signal derived from Cys94, for example, was assigned by the double-labeled Ero1-α in which the carbonyl carbon of cysteine (Cys94) and the nitrogen of glycine (Gly95) were labeled with ^{13}C and ^{15}N, respectively (Fig. S2 B; Serve et al., 2010). NMR signals suggested that Cys94, which is known to accept electrons directly from the a′ domain of PDI, is the most flexible among all cysteines of Ero1-α (Fig. 2 D; Matsunaga et al., 1991; Kim et al., 1994).

Comparing the magnitude of the fluctuations of NMR signals in the presence or absence of PDI, the biggest effect was observed in one signal peak (Fig. 2 E, top middle, asterisk), which was assigned to Cys99 by the selective double-labeling method. This peak disappeared upon addition of somatostatin, a model protein substrate of PDI, which competes for its substrate binding capacity (Fig. 2 E, bottom; Morjana and Gilbert, 1991). Furthermore, a redox-inactive mutant of PDI (PDI(AA)), in which both CXXC motifs in a and a′ domains of PDI are mutated to AXXA, did not affect NMR spectral fluctuations of Ero1-α Cys99, suggesting the redox dependence on the interaction with PDI (Fig. 2 E, bottom middle). Cys99 of Ero1-α is the shuttle cysteine that receives electrons from Cys94 and transfers them to active site cysteine residues (Cys394 and Cys397) during the oxidation of PDI (Fig. 2 D; Araki and Inaba, 2012). Cys99 is also reported to be involved in the regulation of Ero1-α by PDI (Fig. S1 E). Thus, these results suggest that the PDI-induced mobilization of Cys99 will not only allow rearrangement of the Cys94-Cys131 regulatory disulfide bond to activate Ero1-α but also accelerate intramolecular electron transfers within Ero1-α.

Accelerated oxidation of oxidoreductases through the Ero1-α–PDI pathway

Given the evidence for an Ero1-α and PDI hub, we sought to determine whether it can interface productively with other oxidoreductases to promote substrate oxidation (Fig. 3 A). Therefore, we further examined whether PDI could promote Ero1-α–mediated oxidization of other client oxidoreductases. The constitutively active Ero1-α(C104A/C131A) was used to eliminate the effect of Ero1-α activation by PDI (Fig. 2, A and B). Oxygen consumption by Ero1-α coupled with various oxidoreductases was examined in the presence or absence of PDI.

PDI alone or ERp46 alone showed oxygen consumption by Ero1-α(C104/C131A) in the presence of GSH (Fig. 3 B, blue line indicates PDI and green line indicates ERp46). If Ero1-α

adenine dinucleotide [FAD]). Dashed arrows indicate the electron transfer pathway. The four-helix core is shown as a cylinder. (E) ^{13}C NMR spectra of the constitutively active Ero1-α(C104A/C131A) selectively labeled with ^{13}C at the carbonyl carbons of cysteine residues (Ero1*). Spectra were measured in the absence (top) and presence of equimolar amounts of WT PDI (top middle), PDI(AA) mutant (bottom middle), or WT PDI together with 4.25 mM somatostatin (bottom). The spectrum of the unlabeled protein has been subtracted. The asterisk indicates the peak originating from Cys99. A.U., arbitrary unit.

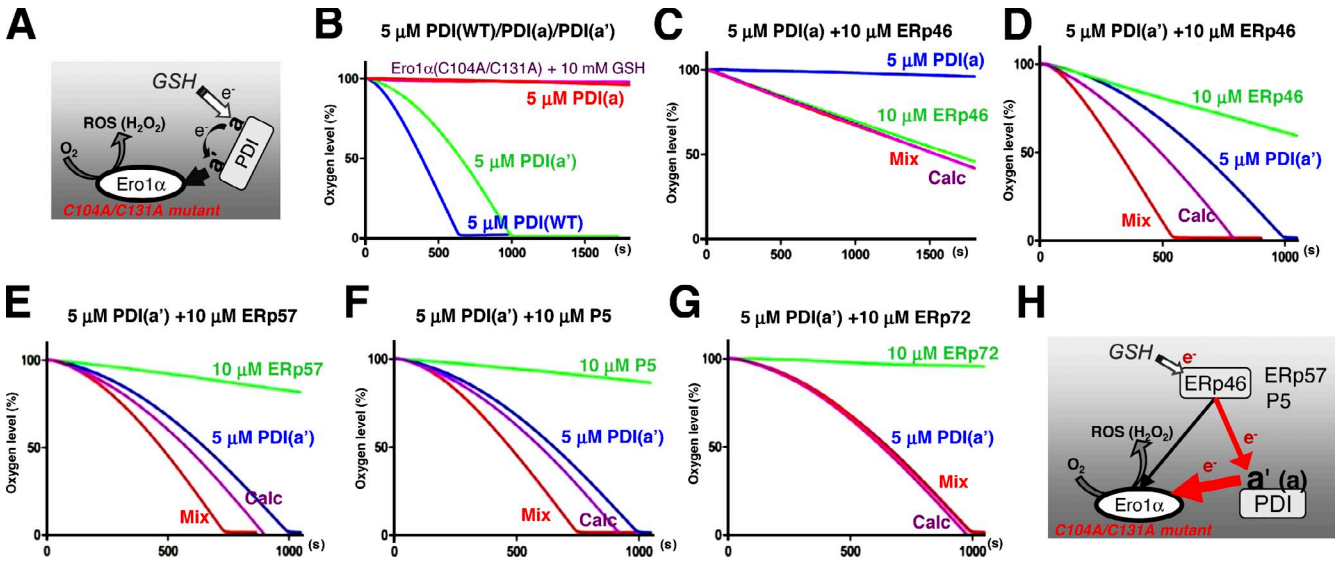

Figure 4. **Synergistic effect is mediated by the a′ domain of PDI.** (A) Schematic model of electron transfer relays between Ero1-α and PDI. Ero1-α oxidizes the a′ domain of PDI, which in turn oxidizes the a domain internally. The oxidized a domain is rereduced by GSH. (B) Kinetics of oxygen consumption by 2 μM constitutively active Ero1-α(C104A/C131A) during the reaction with 5 μM human PDI variants, as depicted in the figure, in the presence of 10 mM GSH. (C–G) Oxygen consumption was assayed in the presence of 10 mM GSH and 10 μM ERp46 (C) with or without 5 μM PDI(a) or 10 μM ERp46 (D), ERp57 (E), P5 (F), or ERp72 (G) with or without 5 μM PDI(a′). Calc shows the calculation data from individual consumption rates of these oxidoreductases. Mix represents the actual consumption rates under conditions in which 10 μM of each oxidoreductase and 5 μM PDI were mixed in the presence of 10 mM GSH. (H) Schematic model of electron transfer relays among Ero1-α, the a′ domain of PDI, and oxidoreductases (ERp46, ERp57, and P5). ROS, reactive oxygen species.

oxidized ERp46 and PDI independently, the oxygen consumption should be additive when both PDI and ERp46 are combined in the reaction mixture (Fig. 3 B, modeled by the purple line, labeled Calc). However, the measured oxygen consumption (Fig. 3 B, red line) was greater than this theoretical consumption curve. Similar, but more modest, synergism with PDI was observed for ERp57 and P5 (Fig. 3, C and D) but not ERp72 (Fig. 3 E). Synergism was not observed for other pairs of oxidoreductases (e.g., ERp57 and P5; Fig. 3 F), suggesting that the core complex composed of Ero1-α and PDI is necessary for the accelerated oxidation of other oxidoreductases. Redox-inactive mutant of PDI (PDI(AA)) did not accelerate the oxygen consumption rate, indicating the synergistic effect of PDI is mediated by its redox activity rather than its chaperone activity or allosteric effects (Fig. S3). Thus, the synergism afforded by the presence of both PDI and other oxidoreductase suggests that the oxidation of PDI by Ero1-α was coupled to successive oxidation of downstream oxidoreductases.

Electron transfer cascade requires the a′ domain of PDI

As we previously reported, electrons are transferred intramolecularly within PDI during its oxidation by Ero1-α (Fig. 4 A; Araki and Nagata, 2011a). To address whether the intramolecular electron transfer also plays a role in the synergistic oxidation mediated by the Ero1-α–PDI pathway, the oxygen consumption assay was again conducted in the presence of PDI mutants, PDI(a′) or PDI(a) (Fig. 2 C), together with the constitutively active Ero1-α(C104A/C131A).

As previously reported, PDI(a) itself was scarcely oxidized by Ero1-α(C104A/C131A) directly (Fig. 4 B) and showed no significant synergistic effect on the oxidation of ERp46 by Ero1-α (C104A/C131A) (Fig. 4 C; Araki and Nagata, 2011a). On the contrary, PDI(a′) was not only oxidized by Ero1-α(C104A/C131A) but also exerted synergistic oxygen consumption in the presence of ERp46 and Ero1-α(C104A/C131A) (Fig. 4, B and D). This synergistic activation of oxygen consumption was similarly observed for other oxidoreductases, including ERp57 and P5 (Fig. 4, E and F), but not for ERp72 (Fig. 4 G). Therefore, the intramolecular electron relay from the a to the a′ domain of PDI appears not to be crucial for the synergism observed in the presence of downstream oxidoreductases. Collectively, the results indicate that electrons are directly transferred from oxidoreductases such as ERp46 to the a′ domain of PDI, and from there to Ero1-α, without passing through the a domain (Fig. 4 H).

To explore the mechanism of the synergism, we further conducted the NMR analysis in the presence of PDI(a′). Interestingly, the a domain inactive mutant of PDI (PDI(a′)) did not induce the flexibility of Cys99 (Fig. 5 C), despite synergistically oxidizing downstream oxidoreductases (Fig. 4, D–F). Considering that WT PDI had a synergistic effect and facilitated mobilization of Cys99 depending on its redox activity, the redox activity of the a domain in addition to the a′ domain might be required for the accelerated mobilization of Cys99 (Fig. 5 B), which suggests that the transfer of electrons from the a domain to the a′ domain of PDI is required for its mobilization. Here, we hypothesized that ERp46 has an equivalent role as the electron donor to the a′ domain of PDI, which was examined by the NMR analysis in the presence of both ERp46 and PDI(a′). Though the overall NMR signals diminished as a result of the hypomobility caused by the increased mass of the complexes, the signal of Cys99 was increased almost to the same level as Cys94 by the presence of ERp46 (compare Fig. 5, E with B), suggesting that ERp46 could substitute for the a domain of PDI

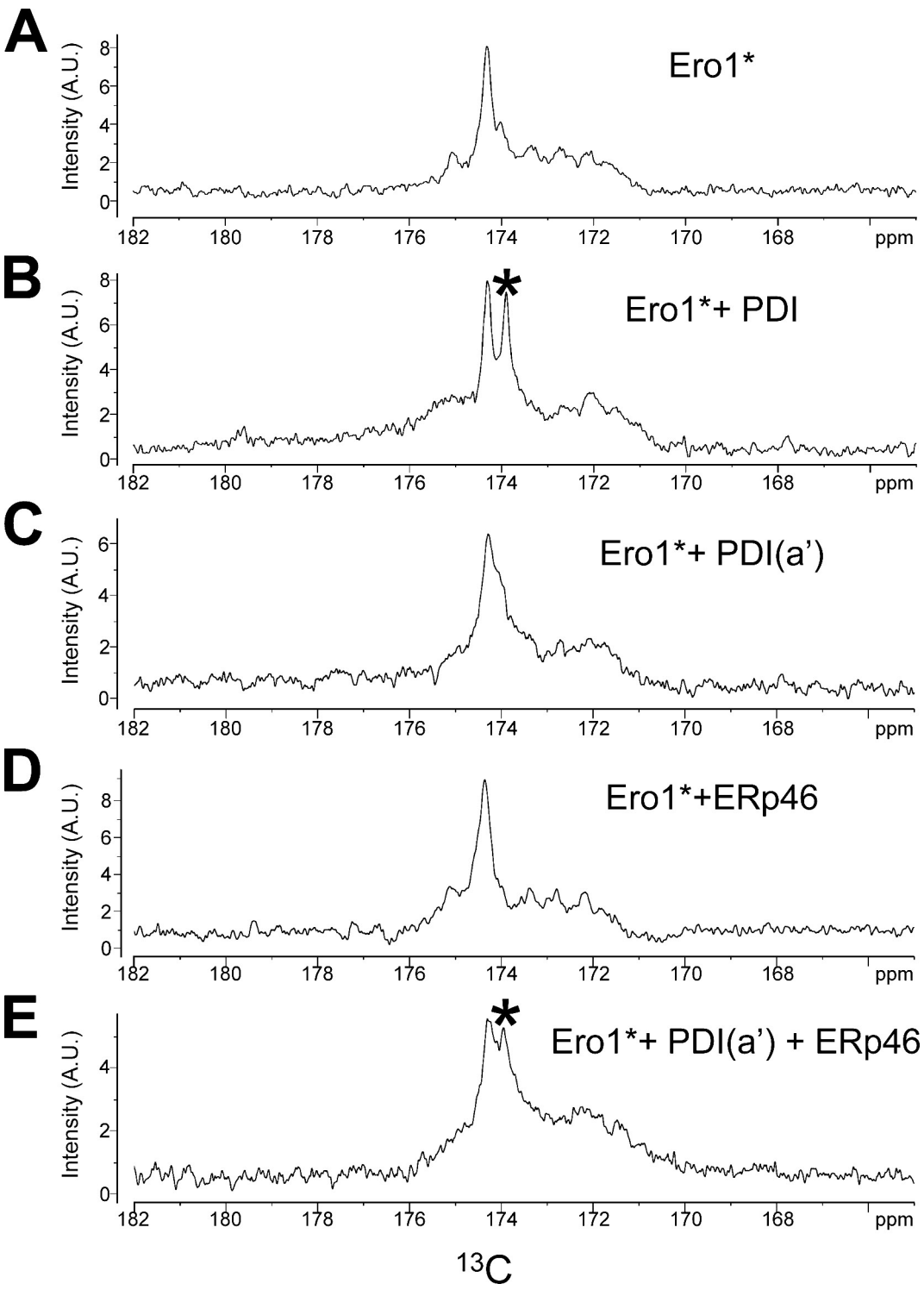

Figure 5. **ERp46 substitutes for the a domain of PDI and increases conformational flexibility in a shuttle cysteine, Cys99, of Ero1-α.** ^{13}C NMR spectra of the constitutively active Ero1-α(C104A/C131A) labeled with ^{13}C selectively at the carbonyl carbons of cysteine residues (Ero1*). (A–E) Spectra were measured in the absence (A) and presence of equimolar amounts of PDI (B), PDI(a′) (C), ERp46 (D), or PDI(a′) and ERp46 (E). Spectrum of the unlabeled protein has already been subtracted. PDI(a′) or ERp46 had no apparent effect on the mobilization of Cys99. The asterisk indicates the peak originating from Cys99. A.U., arbitrary unit.

in terms of electron transfer, resulting in mobilization of Cys99. As a control, ERp46 alone had no apparent effect on the mobilization of Cys99 (Fig. 5 D). Hence, these observations support the notion of sequential and nonconventional electron transfer pathway among oxidoreductases.

Electron transfer cascade in cell

To test whether the electron transfer cascades suggested correlate with events in living cells, we studied direct interactions between oxidoreductases using CXXA mutants as baits to trap substrate protein in mixed disulfides. Proteins trapped by a

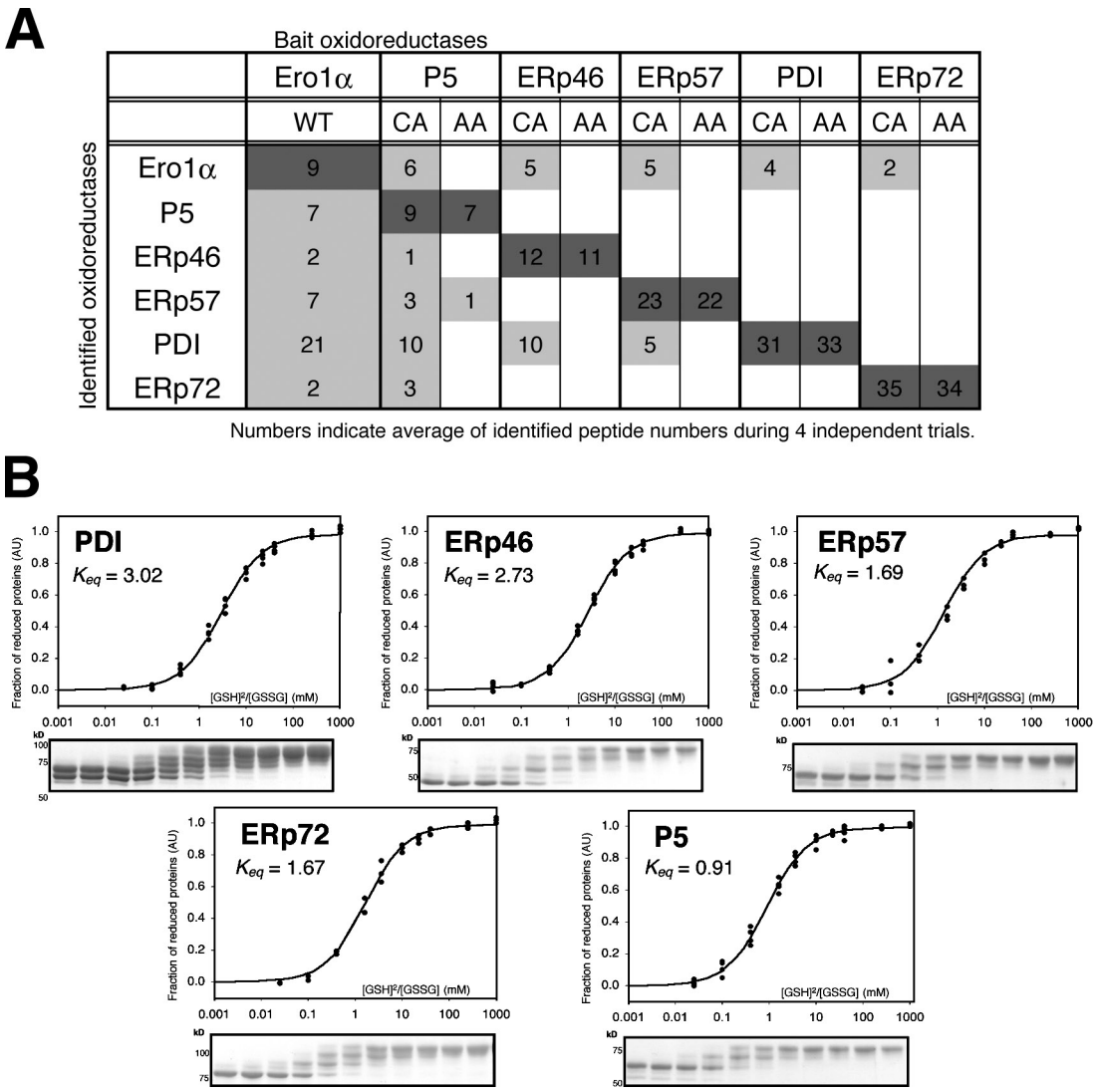

Figure 6. **PDI works as a penultimate electron acceptor in the Ero1-α–mediated oxidation cascade.** (A) Oxidoreductase mutants (CA or AA) and Ero1-α(WT) with FLAG tag were expressed in HEK293T cells, and anti-FLAG immunoprecipitates were analyzed by direct nanoflow liquid chromatography coupled with tandem mass spectrometry. Reproducibly identified oxidoreductases from four independent trials are listed. Each number indicates the identified peptide number of each protein in an individual experiment. Light and dark shading indicate identified prey and bait peptides, respectively. (B) Free sulfhydryl groups of the cysteine residues were modified with mPEG2000-mal after incubation with different $[GSH]^2/[GSSG]$ ratios in a buffer containing 0.1 mM GSSG and varying concentrations of GSH (0.05–10 mM) under a nonoxidative atmosphere at 25°C followed by SDS-PAGE and CBB staining. The apparent equilibrium constants between oxidoreductases and glutathione were determined by the nonlinear least square fitting of the data (Fig. S4, A–D). K_{eq} values were determined from at least three independent trials as follows: 3.02 ± 0.14 (PDI, correlation coefficient: 0.985), 2.73 ± 0.10 (ERp46, 0.994), 1.69 ± 0.12 (ERp57, 0.991), 1.67 ± 0.08 (ERp72, 0.994), and 0.91 ± 0.04 (P5, 0.995). A.U., arbitrary unit.

CXXA mutant are presumed to be the electron recipients in the interaction and can be regarded as downstream components in the electron transport chain (Hatahet and Ruddock, 2007). Coimmunoprecipitation with the constructs listed in Fig. 6 A was followed by mass spectrometry analysis to identify disulfide-linked interacting partners. AXXA active site–null mutants were used as the control for nonredox-based interactions. The resulting data, which were reproducible in four independent experiments, are shown in Fig. 6 A. The CXXA mutant of PDI interacted only with Ero1-α, whereas CXXA mutants of other oxidoreductases interacted with both PDI and Ero1-α. These findings suggest that PDI is the penultimate electron acceptor in a cascade consisting of multiple oxidoreductases. The CXXA mutant of ERp72 interacted with Ero1-α, but WT ERp72 was uniquely inert with Ero1-α and did not show any synergism; thus, this property might be because ERp72 binds to Ero1-α in an active site–independent manner (Fig. 1, D and E). Although the proteomic method could not distinguish direct or indirect interactions between oxidoreductases within the cells, the estimated directions of electron flow among the oxidoreductases were all consistent with the demonstrated synergistic oxidation of oxidoreductases by the Ero1-α–PDI cascade.

Redox equilibrium constants and the electron transfer cascades

To further corroborate the electron transfer between oxidoreductases, the redox equilibrium constant of each enzyme was determined by incubating purified recombinant proteins in redox

buffers containing different ratios of [GSH] to [GSSG]. We monitored the number of free cysteines by modification with mPEG2000-mal (methoxy polyethylene glycol 2000 maleimide) and detecting the shift in mobility by SDS-PAGE and protein staining (Fig. 6 B, bottom panel of each titration curve). Titration curves drawn from the stained gel provided apparent redox equilibrium constants for each oxidoreductase. Because the enzymes in question have more than one active site, these values provide a mean for the whole molecule, which may include cysteines that are not part of the active site (the detailed procedures are provided in Fig. S4; Lundström and Holmgren, 1993; Frickel et al., 2004). Among the oxidoreductases examined, PDI showed the highest redox equilibrium constant (K_{eq} = 3.02). This value is similar to the previously reported constant of K_{eq} = 3.0, supporting the validity of our method (Lundström and Holmgren, 1993; Chambers et al., 2010). The redox equilibrium constant for PDI was slightly higher than that for ERp46 and significantly higher than those for other oxidoreductases, including ERp57, ERp72, and P5. This finding suggested that, once PDI is oxidized preferentially by Ero1-α, it has the potential for returning to the reduced state by oxidizing client proteins, including other oxidoreductases, i.e., receiving electrons from the lower redox equilibrium group of oxidoreductases. These observations are consistent with the proteomics analysis and synergistic oxidation (Fig. 3, Fig. 4, and Fig. 6 A).

Discussion

Our observations suggest a cooperative redox network of ER-resident oxidoreductases sustained by a hierarchy of physical affinities and thiol redox equilibria, centering on the PDI–Ero1-α complex. The biological significance of this oxidative relay via the PDI–Ero1-α complex is assumed to provide prompt on-demand oxidative equivalents to oxidoreductases. Considering the broader context of ER physiology, such as when efficient production of disulfide bond-rich substrates is required, PDI oxidized by Ero1-α is mobilized for the oxidization of other oxidoreductases, which would also be subject to direct oxidization by Ero1-α (Fig. 3). PDI would participate cooperatively in these folding processes as well as in providing an oxidative source. In addition, PDI would recognize the redox state of the ER via direct binding to oxidoreductases, rather than depending on versatile redox buffers, and would modulate the redox state of oxidoreductases optimally by regulating the activity of Ero1-α (Fig. 2, A and B). Substrate specificity of oxidoreductases in the ER should also be taken into account when considering these synergistic oxidation systems. Although the substrate specificity is not yet been fully understood, various oxidoreductases might be required to catalyze the oxidative folding of various types of nascent polypeptides. Disulfide relays to specific substrates of oxidoreductases might need to be shielded from GSH-mediated reduction by means of "kinetic funneling." These possibilities should be experimentally considered in the future.

We uncovered a novel role for the a′ domain of PDI, which accepts electrons directly from other oxidoreductases, such as ERp46, during oxidation by the Ero1-α–PDI complex (Fig. 4). If the a′ domain is efficiently reduced by a reductant such as GSH directly, the a′ domain does not need to receive electrons from the a domain of PDI, and the PDI lacking the a domain would be oxidized as efficiently as PDI(WT) by Ero1-α in the presence of GSH. Apparently, this was not the case (Fig. 4 B; also see Araki and Nagata, 2011a). As previously reported, the biochemical properties, including redox potentials and oxygen consumption rates, are almost identical between the a domain alone and the a′ domain alone (Chambers et al., 2010; Inaba et al., 2010). Collectively, when Ero1-α forms a complex with PDI, the a′ domain of PDI may undergo spatial or conformational changes that restrict access to this domain by small molecules such as GSH (Appenzeller-Herzog et al., 2010; Araki and Inaba, 2012).

Recent studies suggest that PDI dynamically changes its structure via conformational changes around the b′xa′ domains, depending on the redox state of the a′ domain (Nakasako et al., 2010; Serve et al., 2010; Wang et al., 2012). Specifically, PDI remains in the open form when the a′ domain is oxidized but adopts the closed form when the a′ domain is reduced. Considering this conformational change, we propose the following model for the synergistic effect (Fig. 7 A). When PDI is fully reduced, PDI remains in the closed form and interacts relatively stably with Ero1-α (Masui et al., 2011). Ero1-α, once activated, oxidizes the a′ domain of PDI preferentially (Fig. 7 A, i). Immediately afterward, the oxidized a′ domain oxidizes the a domain intramolecularly, resulting in the reduced state (Fig. 7 A, ii), and then, the reduced a′ domain of PDI is subsequently oxidized by Ero1-α, leading to a fully oxidized and open form (Fig. 7 A, iv; Wang et al., 2012, 2013). The oxidized a domain of PDI is reduced mostly by GSH (Fig. 7 A, vi). In an alternative pathway, the oxidized a′ domain of PDI, which may couple with conformational change into open state (Fig. 7 A, iii), can be reduced either by reduced ERp46 or GSH (Fig. 7 A, v and vii). This is because the open state of PDI allows it to access and interact with ERp46 or GSH, whereas the a′ domain of the reduced/closed form of PDI is spatially protected from the solvent (GSH), as mentioned in the previous paragraph. The synergistic effect is derived mostly from processes linked to the ERp46-driven reduction of the a′ domain of PDI (Fig. 7 A, v and vii). ERp46 may be recognized as a substrate of PDI, thereby accelerating the conformational change and rereduction of PDI (Fig. 5). Regarding the a domain mutant variant PDI(a'), Fig. 7 A, iv and v (red color lines), are the main processes, and the synergistic effect is predicted to be derived from these processes (Fig. 7 A, v). Because of the lack of a GSH-driven reduction process (Fig. 7 A, vi), the presence of ERp46 would be expected to have a more marked effect on the reduction of PDI(a′) than on the reduction of PDI(WT). Consistent with this observation, the synergistic effect was more pronounced with PDI(a′) than with PDI(WT) (compare Fig. 3 with Fig. 4). ERp57 and P5 would be also oxidized in a similar fashion to that of ERp46 (Fig. 3 and Fig. 4).

NMR analysis revealed that Cys94 of Ero1-α was the most flexible cysteine, even though Cys94 and Cys99 make disulfide bonds with each other under the activated condition (Fig. S1 E). Intriguingly, Cys99 of Ero1-α showed increased flexibility in the presence of PDI (Fig. 2 E). More interestingly, this mobilization

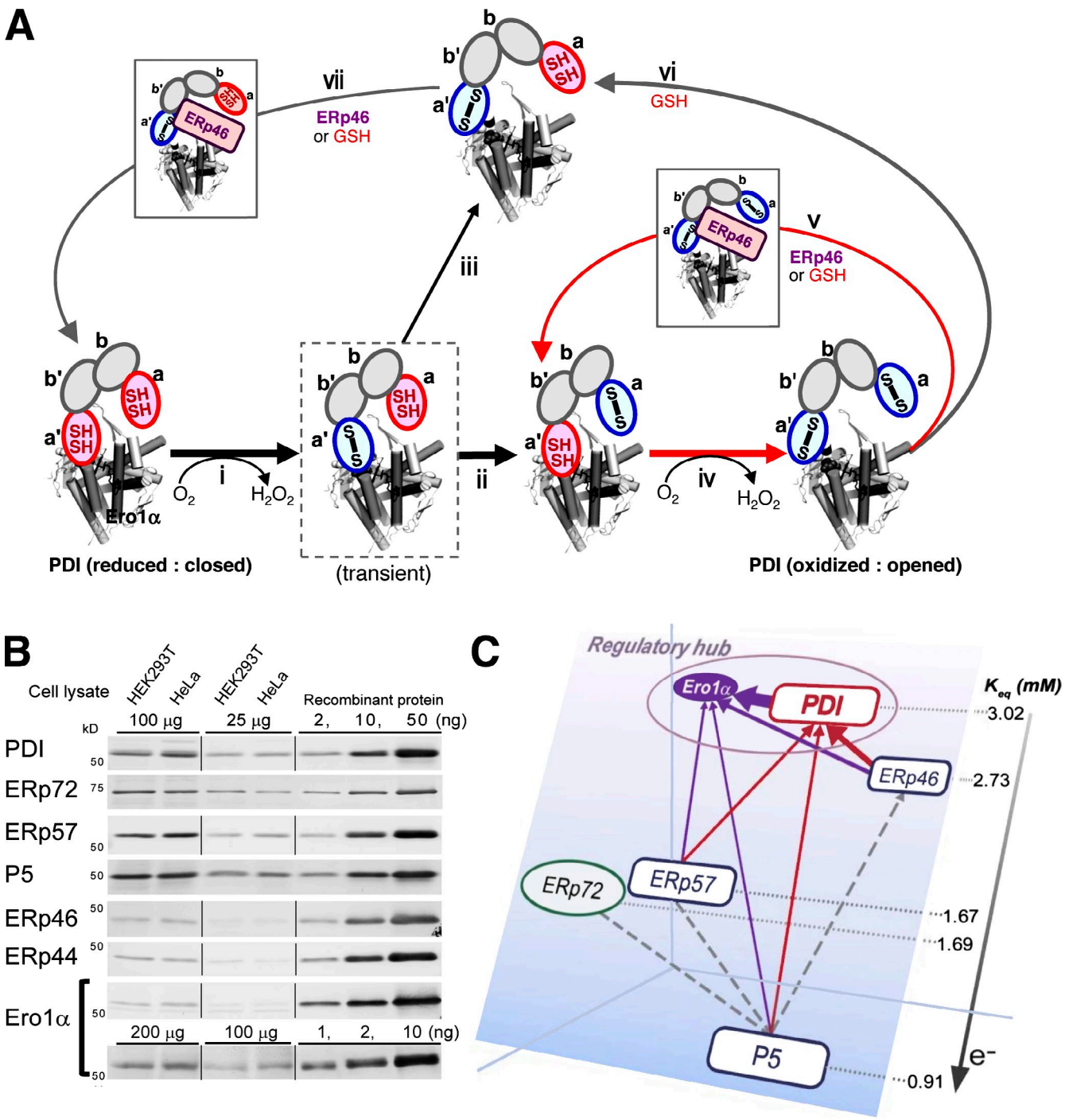

Figure 7. **Model of inter- and intramolecular electron transfer cascade among ER oxidoreductases.** (A) Proposed model for the synergistic effect. Details are described in the Discussion. ERp57 and P5 could be oxidized in a similar fashion to that of ERp46. (B) The intracellular amounts of several ER oxidoreductases in HEK293T or HeLa cells were roughly estimated by immunoblot analysis using the appropriate antibodies, with parallel loading of recombinant proteins on the same gel. The intracellular amounts of PDI, ERp57, P5, and ERp72 were roughly similar, but those of ERp46 and ERp44 were about one fifth of the former. The amount of Ero1-α was only one tenth that of PDI. Black lines indicate the removal of intervening lanes from some of the gels for presentation purposes. (C) Proposed model for electron transfer cascades among the ER oxidoreductases. Red and purple arrows indicate the directions of electron transport. Broken line or arrows indicate a nonredox-based interaction or presumed electron transport, respectively. The apparent redox equilibrium constants are from Fig. 6 B. The relative intracellular amounts of these oxidoreductases are indicated by the box sizes.

of Cys99 required both of the active sites of PDI or additional redox active factors such as ERp46 when the active a domain of PDI was absent (Fig. 5 E). Because no electron donors such as GSH or DTT were present, NMR analysis revealed the equilibrium states of the electron exchanges between Ero1-α, PDI, and ERp46. ERp46 by itself did not accelerate the mobilization of Cys99 (Fig. 5 D). Also, allosteric effects or the chaperone activity of PDI do not appear to be required because PDI(AA) showed no synergistic effect (Fig. S3). Thus, the addition of ERp46 substituted for the role of the a domain of PDI, and

electrons were transferred from ERp46 to the a′ domain of PDI (Fig. 7 A, v), leading to improved Cys99 flexibility. This mobilization of Cys99 would facilitate intramolecular electron relays in Ero1-α from shuttle disulfides (Cys94-Cys99) to the active site disulfides (Cys394-Cys397). This kind of effect might be related to the redox-active center rearrangement identified in *Escherichia coli* DsbB-DsbA (Inaba et al., 2006, 2009; Zhou et al., 2008).

We also estimated the intracellular amounts and the redox equilibrium constants of oxidoreductases in cells (Fig. 7 B). The amount of Ero1-α was roughly one tenth of that of PDI, suggesting that most of the Ero1-α molecules in the cell could be regulated by PDI (van Anken et al., 2009; Tavender et al., 2010). Considering that the redox equilibrium constant of PDI is higher than that of other oxidoreductases, the oxidation reactions via which PDI oxidizes other oxidoreductases seem thermodynamically unfavorable (Fig. 6 B). However, if the redox equilibrium constant of PDI were lower than that of other oxidoreductases, PDI, once oxidized by Ero1-α, would oxidize other oxidoreductases more extensively, and the redox states of other oxidoreductases would not be properly regulated. In keeping with this thermodynamic viewpoint, the synergistic effect was significantly more prominent in the presence of ERp46 and PDI than in the presence of ERp57 or P5 because the redox equilibrium constant of ERp46 is closer to that of PDI than to that of ERp57 or P5 (Fig. 3 and Fig. 4). Therefore, based on the slope of their individual redox equilibrium constants, we could propose an elaborate ER redox network governing oxidoreductases (Fig. 7 C). The fundamental features of the regulatory function of ER oxidoreductases revealed in this work should help provide a basic framework for understanding essential biological processes involving oxidative protein folding and the protein quality control system in the ER (Bánhegyi et al., 2008; Zhang and Kaufman, 2008; Tabas and Ron, 2011).

Materials and methods

Cell culture and antibodies

Human embryonic kidney (HEK293T) and HeLa cells were cultured in DMEM with 10% FBS. The antibodies used in this study were obtained from StressGen (PDI, SPA890; ERp72, SPS720; and ERp57, SPA-725), Abcam (P5, ab37756), Santa Cruz Biotechnology, Inc. (GAPDH, sc-32233; and ERp46, sc-49660), Cell Signaling Technology (ERp44, #2886; PDI, #2446; and ERp57, #2881), Abnova (Ero1-α, H00030001-M01), EMD Millipore (GAPDH, MAB374), and Sigma-Aldrich (FLAG M2). The anti-ERp44 antibody (B68) was the gift from R. Sitia (Università Vita-Salute San Raffaele Scientific Institute, Milan, Italy). Secondary antibodies were obtained from Jackson ImmunoResearch Laboratories, Inc.

Constructs and mutagenesis

The cDNAs of human oxidoreductases (except ERp46), with a C-terminal FLAG tag sequence located just before the ER retention motifs, were PCR amplified from a Matchmaker Pretransformed Human HeLa Library (Takara Bio Inc.) and subcloned into pcDNA3.1 (Ushioda et al., 2008). The human ERp46 cDNA clone (DNA Data Bank of Japan number AK075291) was supplied by the National Biological Resource Center, Department of Biotechnology, National Institute of Technology and Evaluation.

To express the recombinant oxidoreductases, unless otherwise mentioned, full-length peptides without signal sequences and ER-retention motifs were subcloned into the modified pETDuet-1 vector (EMD Millipore), which was modified with an N-terminal 6×His tag and tobacco etch virus protease recognition site. The cysteine to alanine mutations in the oxidoreductases were created using the site-directed mutagenesis kit (QuikChange; Agilent Technologies). All constructs were verified by sequencing.

Cell transfections and stable cell lines

Transfections of cells with plasmids and siRNAs were performed using Effectene (QIAGEN) and RNAiMAX (Invitrogen), respectively. For the siRNA experiments, predesigned siRNAs (Stealth RNAi; Invitrogen) specific for human ER-resident oxidoreductases (Fig. S2 A) were synthesized. Stealth RNA Negative Control Low GC or Negative Control Medium GC was used as a negative control. Stable cell lines expressing FLAG-tagged human Ero1-α(WT) were generated by transfecting pcDNA3.1/Ero1-α(WT)-FLAG into HEK293T cells and selecting for stably transfected clones with 1 mg/ml G418 (Nacalai Tesque).

Proteomics analysis

HEK293T cells were transfected with human PDI family cDNAs using Lipofectamine 2000 (Invitrogen) according to the manufacturer's protocol. At 24 h after transfection, the cells were washed once with PBS containing 20 mM *N*-ethylmaleimide (NEM) and lysed with lysis buffer (20 mM Hepes, pH 7.5, 150 mM NaCl, 20 mM NEM, 50 mM NaF, 1 mM Na_3VO_4, 0.5% digitonin, 1 mM PMSF, 5 µg/ml leupeptin, 5 µg/ml aprotinin, and 3 µg/ml pepstatin A). After centrifugation, the supernatant was incubated with anti-FLAG M2-agarose beads (Sigma-Aldrich) for 1 h, and the beads were washed twice with wash buffer (10 mM Hepes, pH 7.5, 150 mM NaCl, and 0.1% Triton X-100). The immunoprecipitants were eluted with a FLAG peptide (0.5 mg/ml; Sigma-Aldrich) dissolved in wash buffer. After concentration by TCA precipitation, the eluate was redissolved in guanidine hydrochloride and digested with lysyl endopeptidase (Lys-C; Wako Chemicals USA).

All samples were analyzed on a direct nanoflow liquid chromatography system coupled to a time-of-flight mass spectrometer (Q-STAR XL; AB Sciex). The mass spectrometry and tandem mass spectrometry spectra were obtained in information-dependent acquisition mode and were queried against the NCBI nonredundant database with an in-house Mascot server (version 2.2.1; Matrix Science; Natsume et al., 2002). Proteins that were identified by two or more peptides with a peptide expectation value of $P < 0.05$ were considered as reliable identifications.

Protein expression and purification

Overexpression and purification of Ero1-α(WT) and Ero1-α(C104A/C131A) were performed essentially as described previously (Araki and Nagata, 2011a). In brief, Ero1-α and its mutant were overexpressed in *E. coli* BL21(DE3) (EMD Millipore). Cells were grown at 37°C in Luria-Bertani medium containing 100 µg/ml ampicillin and 10 µM flavin adenine dinucleotide to an OD (600 nm) of 0.6, and the expression of the recombinant proteins was induced at 24°C for 12–16 h by adding 200 µM IPTG. Cells were collected, and protein purification was performed at 4°C as follows. Harvested cells were sonicated in lysis buffer (20 mM Hepes-NaOH, pH 7.4, containing 150 mM NaCl, 20 mM imidazole, and protease inhibitor mixture without EDTA [Sigma-Aldrich]). The supernatant was loaded onto a HisTrap column (GE Healthcare) and eluted with 0.5 M imidazole after washing the column with lysis buffer. The eluted sample was oxidized with the addition of potassium ferricyanide at a final concentration of 20 mM for 20 min on ice, which was followed by gel-permeation chromatography (HiLoad 16/60 Superdex 200 prep-grade column; GE Healthcare) preequilibrated with gel buffer (20 mM Hepes-NaOH, pH 7.4, containing 150 mM NaCl). The fractions containing the monomeric form were applied onto the Resource Q column (GE Healthcare) preequilibrated with 20 mM Hepes-NaOH, pH 8. The sample was eluted with a linear NaCl gradient ranging from 0 to 500 mM. Purified proteins were concentrated and stored at −80°C. Other oxidoreductases and their mutants were expressed in *E. coli* BL21(DE3) cells. Expression was induced with 0.3 mM IPTG at 30°C for 6 h just after the OD_{600} reached 0.6. Harvested cells were sonicated in lysis buffer. The supernatant of the cell lysate was loaded onto a HisTrap column equilibrated with lysis buffer and eluted with the same buffer containing 0.5 M imidazole. The elution fractions were loaded onto a HiLoad 16/60 Superdex 200 prep-grade column equilibrated with gel buffer. Eluted fractions containing oxidoreductases were desalted and loaded onto a Resource Q column equilibrated with 20 mM Tris-HCl, pH 8.0. Fractions were eluted with a linear gradient of NaCl. ERp72 and its mutant recombinant proteins were further desalted and purified using a Resource S column (GE Healthcare) equilibrated with 20 mM MES, pH 5.5, and fractions were eluted with a linear gradient of NaCl. Again, purified proteins were concentrated and stored at −80°C.

Immunoprecipitation of FLAG-tagged oxidoreductases or endogenous Ero1-α

Proteins of transfected cells were alkylated by incubation with PBS containing 30 mM NEM (Wako Chemicals USA) for 30 min on ice. Cells were

extracted in lysis buffer (50 mM Hepes-NaOH, pH 7.5, containing 150 mM NaCl, 1% Nonidet P-40, 20 mM NEM, and protease inhibitors) and centrifuged at 15,000 *g* for 20 min at 4°C. The supernatants were used for immunoblotting, for immunoprecipitation of FLAG-tagged oxidoreductases with anti-FLAG M2-agarose beads (Sigma-Aldrich; 1), or for immunoprecipitation of endogenous Ero1-α with Con A–Sepharose 4B (GE Healthcare; 2). Bead suspensions were rotated for 3 h at 4°C. After precipitation, the beads were washed three times with lysis buffer and eluted by adding lysis buffer containing 0.2 mg/ml FLAG peptide for 1 or by denaturing with SDS-PAGE sample buffer containing 5 mM EDTA for 2. Immunoblotting was conducted under reducing or nonreducing conditions with specific antibodies as indicated in the text (Results section Ero1-α is dominantly regulated by PDI).

SPR measurements

The SPR analysis was performed essentially as described previously (Araki and Nagata, 2011a). In brief, association or dissociation rate constants (k_{on} or k_{off}) for the direct binding of oxidoreductases to immobilized Ero1-α(WT) were determined by SPR measurements on a protein interaction array system (ProteOn XPR36; Bio-Rad Laboratories). Ero1-α(WT) was coupled to the GLC (general amine coupling, compact polymer layer) sensor chip (Bio-Rad Laboratories) through amine-coupling chemistry. As a control, one channel was coupled with BSA to exclude background binding. Sensorgrams were recorded simultaneously for five concentrations of purified oxidoreductases (0.133–36 µM) in threefold increments at 25°C for a 2-min association phase followed by a 10-min dissociation phase with 20 mM Hepes-NaOH, pH 7.4, 150 mM NaCl, 0.001% Tween, and 2 mM EDTA as running and sample buffers. GSH or GSSG (final 2 mM GSH and 0.5 mM GSSG) were added to the running buffer just before use, and all samples were exchanged and diluted in this buffer. Sensorgrams were analyzed by nonlinear regression analysis according to a two-state model using ProteOn Manager Version 3.0 software (Bio-Rad Laboratories). Experiments were replicated at least three times.

Oxygen consumption assays

Oxygen consumption was measured using a Clark-type oxygen electrode (YSI 5331) as previously described (Araki and Nagata, 2011a). In brief, all experiments were performed at 25°C using a constant temperature incubator in air-saturated buffer (~250 µM O_2) in 50 mM Hepes-NaOH, pH 7.5, 150 mM NaCl, and 2 mM EDTA. Catalytic oxygen consumption was initiated by the addition of Ero1-α(WT) or Ero1-α(C104A/C131A) at a final concentration of 2 µM in a reaction mixture containing 10 mM GSH and various concentrations of oxidoreductases as depicted in each figure.

NMR measurements

E. coli cells were grown in M9 minimal media containing 25 mg/liter L-[1-^{13}C]cysteine, either with or without 100 mg/liter L-[^{15}N]alanine or 200 mg/liter L-[^{15}N]glycine, to produce isotopically labeled constitutively active Ero1-α(C104A/C131A). NMR measurements were made on a research spectrometer (AVANCE III-400; Bruker) at 303 K with a 5-mm NMR sample tube, which contained 0.85 mM Ero1-α(C104A/C131A) dissolved in 10 mM sodium phosphate buffer containing 100 mM NaCl, pH 7.0. ^{13}C NMR spectra were recorded at 100 MHz with a WALTZ-16 composite pulse decoupling sequence. The free induction decay was recorded with 32 K data points and a spectral width of 3,500 Hz. Carbonyl ^{13}C signals were assigned by the selective ^{13}C carbonyl-^{15}N double-labeling method (Serve et al., 2010). The ^{13}CO-^{15}N linkages in the polypeptide chains of the doubly labeled proteins are used to give the carbonyl ^{13}C resonances that split into doublets as a result of the ^{13}C-^{15}N spin coupling (Kainosho and Tsuji, 1982). Thus, one can sort out the carbonyl ^{13}C resonances caused by the amino acid residues that possess a ^{13}CO-^{15}N linkage. If there is only one ^{13}CO-^{15}N linkage in a protein molecule, it is possible to unambiguously assign the carbonyl ^{13}C resonance to the specific amino acid residue on the basis of knowledge of the amino acid sequence of the protein. For example, Cys94 of Ero1-α was assigned by the double-labeled Ero1-α in which the carbonyl carbon of cysteine (Cys94) and the nitrogen of glycine (Gly95) because the Cys-Gly linkage exists only here in the Ero1-α protein sequence. To subtract the signal of the natural isotope abundance, the spectrum of the unlabeled protein was subtracted from that of the labeled one. All data were collected and processed under the same experimental condition, and the y axis indicates relative intensity (arbitrary unit).

Measurement of redox equilibrium using glutathione

The redox equilibrium between recombinant oxidoreductases and glutathione was measured essentially as described previously (Sugiura et al., 2010). In brief, oxidoreductases (1 µM) were incubated with 0.1 mM GSSG and various concentrations of GSH at 25°C for 1 h in 0.1 M sodium phosphate buffer, pH 7.0, containing 1 mM EDTA and 150 mM NaCl. After incubation, 10% TCA was added to prevent further thiol–disulfide exchange. The precipitated pellet was washed with 100% acetone and solubilized in 0.1 M sodium phosphate buffer, pH 7.0, containing 2% SDS and 3 mM methoxypolyethylene glycol (mean molecular weight of 2,000)-maleimide (mPEG2000-mal; Sunbright ME-020MA, NOF Corporation). The mixture was incubated at 25°C for 30 min to alkylate the free sulfhydryl groups of cysteines. Samples were separated by SDS-PAGE and stained with Coomassie brilliant blue (CBB). Values for the reduced form fraction were quantified by measuring the PEG2000-induced mobility from the complete oxidized state as shown in Fig. S4. After quantification, the values for the completely oxidized or reduced states were regarded as 0 or 1, respectively, and all intermediate states were recalibrated. The redox equilibrium constant (K_{eq}) was calculated by fitting the recalibrated fraction of the apparent reduced form to the following equation: $R = ([GSH]^2/[GSSG])/\{K_{eq} + ([GSH]^2/[GSSG])\}$, in which R is the relative ratio of reduced oxidoreductases.

Online supplemental material

Fig. S1 shows that Ero1-α binds to ER-resident oxidoreductases. Fig. S2 shows validation of siRNA silencing and annotation of Cys94 with a double-labeling method. Fig. S3 shows PDI(AA) does not accelerate the Ero1-α oxidation system. Fig. S4 shows the method used to calculate the K_{eq} values. Table S1 shows a list of publications reporting Ero1-α–related assays and having a bearing on this study. Online supplemental material is available at http://www.jcb.org/cgi/content/full/jcb.201303027/DC1.

We thank Ryota Maeda and Yo-ichi Nabeshima for allowing us to use their SPR system. We thank Koreaki Ito for his critical reading of the manuscript and valuable suggestions. We thank Lars Ellgaard for sharing his work before publication and for providing informative suggestions.

This work was supported by a Grant-in-Aid for Creative Scientific Research (19G0314) and for Scientific Research on Priority Area (19058008) from the Ministry of Education, Culture, Sports, Science and Technology (to K. Nagata), Grants-in-Aid for Scientific Research on Innovative Areas (25102008), for Scientific Research (24249002), and partly, Nanotechnology Platform Program from the Ministry of Education, Culture, Sports, Science and Technology (to K. Kato), a Grant-in-Aid for Scientific Research on Priority Areas (22020039; to Y. Kamiya), the New Energy and Industrial Technology Development Organization (to T. Natsume), and a fellowship from the Japan Society for the Promotion of Science (to K. Araki). D. Ron is a Wellcome Trust Principal Research Fellow.

Submitted: 6 March 2013
Accepted: 8 August 2013

References

Anelli, T., M. Alessio, A. Bachi, L. Bergamelli, G. Bertoli, S. Camerini, A. Mezghrani, E. Ruffato, T. Simmen, and R. Sitia. 2003. Thiol-mediated protein retention in the endoplasmic reticulum: the role of ERp44. *EMBO J.* 22:5015–5022. http://dx.doi.org/10.1093/emboj/cdg491

Appenzeller-Herzog, C., and L. Ellgaard. 2008. The human PDI family: versatility packed into a single fold. *Biochim. Biophys. Acta.* 1783:535–548. http://dx.doi.org/10.1016/j.bbamcr.2007.11.010

Appenzeller-Herzog, C., J. Riemer, B. Christensen, E.S. Sørensen, and L. Ellgaard. 2008. A novel disulphide switch mechanism in Ero1alpha balances ER oxidation in human cells. *EMBO J.* 27:2977–2987. http://dx.doi.org/10.1038/emboj.2008.202

Appenzeller-Herzog, C., J. Riemer, E. Zito, K.T. Chin, D. Ron, M. Spiess, and L. Ellgaard. 2010. Disulphide production by Ero1α-PDI relay is rapid and effectively regulated. *EMBO J.* 29:3318–3329. http://dx.doi.org/10.1038/emboj.2010.203

Araki, K., and K. Inaba. 2012. Structure, mechanism, and evolution of Ero1 family enzymes. *Antioxid. Redox Signal.* 16:790–799. http://dx.doi.org/10.1089/ars.2011.4418

Araki, K., and K. Nagata. 2011a. Functional in vitro analysis of the ERO1 protein and protein-disulfide isomerase pathway. *J. Biol. Chem.* 286:32705–32712. http://dx.doi.org/10.1074/jbc.M111.227181

Araki, K., and K. Nagata. 2011b. Protein folding and quality control in the ER. *Cold Spring Harb. Perspect. Biol.* 3:a007526. http://dx.doi.org/10.1101/cshperspect.a007526

Baker, K.M., S. Chakravarthi, K.P. Langton, A.M. Sheppard, H. Lu, and N.J. Bulleid. 2008. Low reduction potential of Ero1alpha regulatory disulphides

ensures tight control of substrate oxidation. *EMBO J.* 27:2988–2997. http://dx.doi.org/10.1038/emboj.2008.230

Bánhegyi, G., J. Mandl, and M. Csala. 2008. Redox-based endoplasmic reticulum dysfunction in neurological diseases. *J. Neurochem.* 107:20–34. http://dx.doi.org/10.1111/j.1471-4159.2008.05571.x

Benham, A.M. 2012. The protein disulfide isomerase family: key players in health and disease. *Antioxid. Redox Signal.* 16:781–789. http://dx.doi.org/10.1089/ars.2011.4439

Benham, A.M., A. Cabibbo, A. Fassio, N. Bulleid, R. Sitia, and I. Braakman. 2000. The CXXCXXC motif determines the folding, structure and stability of human Ero1-Lalpha. *EMBO J.* 19:4493–4502. http://dx.doi.org/10.1093/emboj/19.17.4493

Chambers, J.E., T.J. Tavender, O.B. Oka, S. Warwood, D. Knight, and N.J. Bulleid. 2010. The reduction potential of the active site disulfides of human protein disulfide isomerase limits oxidation of the enzyme by Ero1α. *J. Biol. Chem.* 285:29200–29207. http://dx.doi.org/10.1074/jbc.M110.156596

Dixon, B.M., S.H. Heath, R. Kim, J.H. Suh, and T.M. Hagen. 2008. Assessment of endoplasmic reticulum glutathione redox status is confounded by extensive ex vivo oxidation. *Antioxid. Redox Signal.* 10:963–972. http://dx.doi.org/10.1089/ars.2007.1869

Ellgaard, L., and L.W. Ruddock. 2005. The human protein disulphide isomerase family: substrate interactions and functional properties. *EMBO Rep.* 6:28–32. http://dx.doi.org/10.1038/sj.embor.7400311

Freedman, R.B., T.R. Hirst, and M.F. Tuite. 1994. Protein disulphide isomerase: building bridges in protein folding. *Trends Biochem. Sci.* 19:331–336. http://dx.doi.org/10.1016/0968-0004(94)90072-8

Frickel, E.M., P. Frei, M. Bouvier, W.F. Stafford, A. Helenius, R. Glockshuber, and L. Ellgaard. 2004. ERp57 is a multifunctional thiol-disulfide oxidoreductase. *J. Biol. Chem.* 279:18277–18287. http://dx.doi.org/10.1074/jbc.M314089200

Gross, E., C.S. Sevier, N. Heldman, E. Vitu, M. Bentzur, C.A. Kaiser, C. Thorpe, and D. Fass. 2006. Generating disulfides enzymatically: reaction products and electron acceptors of the endoplasmic reticulum thiol oxidase Ero1p. *Proc. Natl. Acad. Sci. USA*. 103:299–304. http://dx.doi.org/10.1073/pnas.0506448103

Hatahet, F., and L.W. Ruddock. 2007. Substrate recognition by the protein disulfide isomerases. *FEBS J.* 274:5223–5234. http://dx.doi.org/10.1111/j.1742-4658.2007.06058.x

Hatahet, F., and L.W. Ruddock. 2009. Protein disulfide isomerase: a critical evaluation of its function in disulfide bond formation. *Antioxid. Redox Signal.* 11:2807–2850. http://dx.doi.org/10.1089/ars.2009.2466

Hebert, D.N., and M. Molinari. 2007. In and out of the ER: protein folding, quality control, degradation, and related human diseases. *Physiol. Rev.* 87:1377–1408. http://dx.doi.org/10.1152/physrev.00050.2006

Inaba, K., S. Murakami, M. Suzuki, A. Nakagawa, E. Yamashita, K. Okada, and K. Ito. 2006. Crystal structure of the DsbB-DsbA complex reveals a mechanism of disulfide bond generation. *Cell*. 127:789–801. http://dx.doi.org/10.1016/j.cell.2006.10.034

Inaba, K., S. Murakami, A. Nakagawa, H. Iida, M. Kinjo, K. Ito, and M. Suzuki. 2009. Dynamic nature of disulphide bond formation catalysts revealed by crystal structures of DsbB. *EMBO J.* 28:779–791. http://dx.doi.org/10.1038/emboj.2009.21

Inaba, K., S. Masui, H. Iida, S. Vavassori, R. Sitia, and M. Suzuki. 2010. Crystal structures of human Ero1α reveal the mechanisms of regulated and targeted oxidation of PDI. *EMBO J.* 29:3330–3343. http://dx.doi.org/10.1038/emboj.2010.222

Jessop, C.E., S. Chakravarthi, N. Garbi, G.J. Hämmerling, S. Lovell, and N.J. Bulleid. 2007. ERp57 is essential for efficient folding of glycoproteins sharing common structural domains. *EMBO J.* 26:28–40. http://dx.doi.org/10.1038/sj.emboj.7601505

Jessop, C.E., T.J. Tavender, R.H. Watkins, J.E. Chambers, and N.J. Bulleid. 2009a. Substrate specificity of the oxidoreductase ERp57 is determined primarily by its interaction with calnexin and calreticulin. *J. Biol. Chem.* 284:2194–2202. http://dx.doi.org/10.1074/jbc.M808054200

Jessop, C.E., R.H. Watkins, J.J. Simmons, M. Tasab, and N.J. Bulleid. 2009b. Protein disulphide isomerase family members show distinct substrate specificity: P5 is targeted to BiP client proteins. *J. Cell Sci.* 122:4287–4295. http://dx.doi.org/10.1242/jcs.059154

Kainosho, M., and T. Tsuji. 1982. Assignment of the three methionyl carbonyl carbon resonances in *Streptomyces* subtilisin inhibitor by a carbon-13 and nitrogen-15 double-labeling technique. A new strategy for structural studies of proteins in solution. *Biochemistry*. 21:6273–6279. http://dx.doi.org/10.1021/bi00267a036

Kim, H., C. Matsunaga, A. Yoshino, K. Kato, and Y. Arata. 1994. Dynamical structure of the hinge region of immunoglobulin G as studied by 13C nuclear magnetic resonance spectroscopy. *J. Mol. Biol.* 236:300–309. http://dx.doi.org/10.1006/jmbi.1994.1136

Lundström, J., and A. Holmgren. 1993. Determination of the reduction-oxidation potential of the thioredoxin-like domains of protein disulfide-isomerase from the equilibrium with glutathione and thioredoxin. *Biochemistry*. 32:6649–6655. http://dx.doi.org/10.1021/bi00077a018

Masui, S., S. Vavassori, C. Fagioli, R. Sitia, and K. Inaba. 2011. Molecular bases of cyclic and specific disulfide interchange between human ERO1alpha protein and protein-disulfide isomerase (PDI). *J. Biol. Chem.* 286:16261–16271. http://dx.doi.org/10.1074/jbc.M111.231357

Matsunaga, C., K. Kato, and Y. Arata. 1991. A 13C NMR study of the hinge region of a mouse monoclonal antibody. *J. Biomol. NMR*. 1:379–390. http://dx.doi.org/10.1007/BF02192861

Morjana, N.A., and H.F. Gilbert. 1991. Effect of protein and peptide inhibitors on the activity of protein disulfide isomerase. *Biochemistry*. 30:4985–4990. http://dx.doi.org/10.1021/bi00234a021

Nakasako, M., A. Maeno, E. Kurimoto, T. Harada, Y. Yamaguchi, T. Oka, Y. Takayama, A. Iwata, and K. Kato. 2010. Redox-dependent domain rearrangement of protein disulfide isomerase from a thermophilic fungus. *Biochemistry*. 49:6953–6962. http://dx.doi.org/10.1021/bi1006089

Natsume, T., Y. Yamauchi, H. Nakayama, T. Shinkawa, M. Yanagida, N. Takahashi, and T. Isobe. 2002. A direct nanoflow liquid chromatography-tandem mass spectrometry system for interaction proteomics. *Anal. Chem.* 74:4725–4733. http://dx.doi.org/10.1021/ac020018n

Riemer, J., N. Bulleid, and J.M. Herrmann. 2009. Disulfide formation in the ER and mitochondria: two solutions to a common process. *Science*. 324:1284–1287. http://dx.doi.org/10.1126/science.1170653

Rutkevich, L.A., and D.B. Williams. 2012. Vitamin K epoxide reductase contributes to protein disulfide formation and redox homeostasis within the endoplasmic reticulum. *Mol. Biol. Cell*. 23:2017–2027. http://dx.doi.org/10.1091/mbc.E12-02-0102

Rutkevich, L.A., M.F. Cohen-Doyle, U. Brockmeier, and D.B. Williams. 2010. Functional relationship between protein disulfide isomerase family members during the oxidative folding of human secretory proteins. *Mol. Biol. Cell*. 21:3093–3105. http://dx.doi.org/10.1091/mbc.E10-04-0356

Serve, O., Y. Kamiya, A. Maeno, M. Nakano, C. Murakami, H. Sasakawa, Y. Yamaguchi, T. Harada, E. Kurimoto, M. Yagi-Utsumi, et al. 2010. Redox-dependent domain rearrangement of protein disulfide isomerase coupled with exposure of its substrate-binding hydrophobic surface. *J. Mol. Biol.* 396:361–374. http://dx.doi.org/10.1016/j.jmb.2009.11.049

Sevier, C.S., and C.A. Kaiser. 2008. Ero1 and redox homeostasis in the endoplasmic reticulum. *Biochim. Biophys. Acta*. 1783:549–556. http://dx.doi.org/10.1016/j.bbamcr.2007.12.011

Sevier, C.S., H. Qu, N. Heldman, E. Gross, D. Fass, and C.A. Kaiser. 2007. Modulation of cellular disulfide-bond formation and the ER redox environment by feedback regulation of Ero1. *Cell*. 129:333–344. http://dx.doi.org/10.1016/j.cell.2007.02.039

Sugiura, Y., K. Araki, S. Iemura, T. Natsume, J. Hoseki, and K. Nagata. 2010. Novel thioredoxin-related transmembrane protein TMX4 has reductase activity. *J. Biol. Chem.* 285:7135–7142. http://dx.doi.org/10.1074/jbc.M109.082545

Tabas, I., and D. Ron. 2011. Integrating the mechanisms of apoptosis induced by endoplasmic reticulum stress. *Nat. Cell Biol.* 13:184–190. http://dx.doi.org/10.1038/ncb0311-184

Tavender, T.J., and N.J. Bulleid. 2010. Molecular mechanisms regulating oxidative activity of the Ero1 family in the endoplasmic reticulum. *Antioxid. Redox Signal.* 13:1177–1187. http://dx.doi.org/10.1089/ars.2010.3230

Tavender, T.J., J.J. Springate, and N.J. Bulleid. 2010. Recycling of peroxiredoxin IV provides a novel pathway for disulphide formation in the endoplasmic reticulum. *EMBO J.* 29:4185–4197. http://dx.doi.org/10.1038/emboj.2010.273

Ushioda, R., J. Hoseki, K. Araki, G. Jansen, D.Y. Thomas, and K. Nagata. 2008. ERdj5 is required as a disulfide reductase for degradation of misfolded proteins in the ER. *Science*. 321:569–572. http://dx.doi.org/10.1126/science.1159293

van Anken, E., F. Pena, N. Hafkemeijer, C. Christis, E.P. Romijn, U. Grauschopf, V.M. Oorschot, T. Pertel, S. Engels, A. Ora, et al. 2009. Efficient IgM assembly and secretion require the plasma cell induced endoplasmic reticulum protein pERp1. *Proc. Natl. Acad. Sci. USA*. 106:17019–17024. http://dx.doi.org/10.1073/pnas.0903036106

van Lith, M., S. Tiwari, J. Pediani, G. Milligan, and N.J. Bulleid. 2011. Real-time monitoring of redox changes in the mammalian endoplasmic reticulum. *J. Cell Sci.* 124:2349–2356. http://dx.doi.org/10.1242/jcs.085530

Wang, C., J. Yu, L. Huo, L. Wang, W. Feng, and C.C. Wang. 2012. Human protein-disulfide isomerase is a redox-regulated chaperone activated by oxidation of domain a'. *J. Biol. Chem.* 287:1139–1149. http://dx.doi.org/10.1074/jbc.M111.303149

Wang, C., W. Li, J. Ren, J. Fang, H. Ke, W. Gong, W. Feng, and C.C. Wang. 2013. Structural insights into the redox-regulated dynamic conformations of human protein disulfide isomerase. *Antioxid. Redox Signal.* 19:36–45. http://dx.doi.org/10.1089/ars.2012.4630

Wang, L., S.J. Li, A. Sidhu, L. Zhu, Y. Liang, R.B. Freedman, and C.C. Wang. 2009. Reconstitution of human Ero1-Lalpha/protein-disulfide isomerase oxidative folding pathway in vitro. Position-dependent differences in role between the a and a' domains of protein-disulfide isomerase. *J. Biol. Chem.* 284:199–206. http://dx.doi.org/10.1074/jbc.M806645200

Zhang, K., and R.J. Kaufman. 2008. From endoplasmic-reticulum stress to the inflammatory response. *Nature*. 454:455–462. http://dx.doi.org/10.1038/nature07203

Zhou, Y., T. Cierpicki, R.H. Jimenez, S.M. Lukasik, J.F. Ellena, D.S. Cafiso, H. Kadokura, J. Beckwith, and J.H. Bushweller. 2008. NMR solution structure of the integral membrane enzyme DsbB: functional insights into DsbB-catalyzed disulfide bond formation. *Mol. Cell*. 31:896–908. http://dx.doi.org/10.1016/j.molcel.2008.08.028

Zito, E., E.P. Melo, Y. Yang, A. Wahlander, T.A. Neubert, and D. Ron. 2010. Oxidative protein folding by an endoplasmic reticulum-localized peroxiredoxin. *Mol. Cell*. 40:787–797. http://dx.doi.org/10.1016/j.molcel.2010.11.010